Evaluation of the method based on PSR techniques for target detection in reverberation

2009 J. Phys. A: Math. Theor. 42 195004

(http://iopscience.iop.org/1751-8121/42/19/195004)

IOP PUBLISHING JOURNAL OF PHYSICS A: MATHEMATICAL AND THEORETICAL

J. Phys. A: Math. Theor. **42** (2009) 195004 (16pp) doi:10.1088/1751-8113/42/19/195004

Evaluation of the method based on PSR techniques for target detection in reverberation

Huiquan Zhang[1], Bohou Xu[1], Jianlong Li[2] and Zhong-Ping Jiang[3]

[1] Department of Mechanics, State Key Laboratory of Fluid Power Transmission and Control, Zhejiang University, Hangzhou 310027, People's Republic of China
[2] Institute of Information and Communication Engineering, Zhejiang University, Hangzhou 310027, People's Republic of China
[3] Department of Electrical and Computer Engineering, Polytechnic University, Brooklyn, NY 11201, USA

E-mail: xubohou@zju.edu.cn

Received 26 December 2008, in final form 20 February 2009
Published 21 April 2009
Online at stacks.iop.org/JPhysA/42/195004

Abstract

In this paper, we consider the problem of target detection in the presence of sea-bottom reverberation. The method based on parameter-induced stochastic resonance (PSR) is adopted, and the non-Rayleigh properties of reverberation, as well as some random characteristics of target echoes, such as random phase and amplitude, are involved. Numerical simulations are carried out to evaluate the performances of the method based on PSR techniques versus the conventional method. The results show that when the number of scatterers that contribute to the reverberation at the same time becomes smaller, the receiver based on PSR techniques will perform better and be more efficient for reverberation suppression than the conventional receiver.

PACS numbers: 05.40.−a, 02.50.−r

1. Introduction

Since proposed by Benzi *et al* in 1981 to explain the periodicity of ice ages [1, 2], the theory and applications of stochastic resonance (SR) has been an attractive research area [3]. The fact that the output signal-to-noise ratio (SNR) can be larger than the input SNR [4, 5], means that the applications of SR in signal processing, especially in signal detection, have attracted a lot of interest recently [6–8]. It has been shown that some nonlinear suboptimal [9, 10] or optimal [11] detectors can be improved by adding noise, which show the SR effects in signal detection. On the other hand, some nonlinear SR systems, such as static threshold systems, dynamical bistable systems, discrete autoregressive models, static or dynamical saturating systems and the parallel arrays [7, 8, 12] of these subsystems, are inserted before the linear coherent

detector (LCD) [6, 8] to improve the detection performance via adding noise or optimizing system parameters, the latter of which is the basis of parameter-induced SR (PSR) [13, 14]. It was shown that the performance of the LCD in white Gaussian noise cannot be enhanced by SR or PSR techniques [6, 8, 15], because the LCD is already optimal in this case. Nevertheless, more robustness of the bistable/monostable filter to mismatch was observed [7, 16], and the detection enhancements by SR in some non-Gaussian cases have been demonstrated [6, 8].

In this paper, we consider the problem of target detection in the presence of reverberation, which is often encountered in an active sonar system. In the shallow-water environment, the detection of targets on the sea floor is often limited by the bottom reverberation [17]. According to the point-scattering theory [18–20], the reverberation arises from a multitude of scatterers distributed independently on the sea floor. On the assumptions of a very large number of reflectors, the reverberation process has a Gaussian probability density function (PDF) and thus Rayleigh envelope. However, non-Rayleigh reverberation can occur when the conditions of the central limit theory (CLT) are violated [18, 20–22]. For example, there may be too few scatterers in the resolution cell of the high-resolution active sonar systems, or the scatterers may not be identically distributed. The non-Rayleigh reverberation always results in more heavy-tailed envelope PDFs after the matched filter [22], leading to an increase of the probability of false alarm.

In the previous paper [23], we have proposed the method based on PSR techniques for this problem, and only the Rayleigh reverberation was considered. Therefore, we wonder how better the performance of this method is compared to the conventional receiver (a spatial matched filter followed by a LCD) when the reverberation envelope deviates from the Rayleigh distribution. In this paper, the detection performances of the method based on PSR techniques and the conventional receiver are evaluated and compared through numerical simulations. In addition, non-Rayleigh characteristics of the reverberation, as well as random phase and amplitude of the target echo, are involved in this paper. The reverberation is generated according to the point-scatterer simulation method [24], and hence non-Rayleigh reverberation is derived when reducing the number of scatterers. Thus, utilizing the simulated reverberation, the performances of the two receivers can be evaluated with Monte Carlo simulations.

The rest of this paper is organized as follows. In section 2, we give a brief review of the problem of target detection in bottom reverberation, together with the conventional resolution and that based PSR techniques for such a problem. Numerical simulations are carried out in section 3. The point-scatterer simulation method for reverberation generation is presented, and the results of Monte Carlo simulations as well as some comments are given. Finally, conclusions are made in section 4.

2. The detection problem and its resolutions

2.1. The problem of target detection in bottom reverberation

Assume that the transmitter emits a pure-tone pulse signal using a non-directive source with the frequency f_0 (Hz) and duration T (s). There is a target body on the bottom at the range $R \gg h$ as shown in figure 1, where h is the depth of the sea. Here we assume that the specular reflection of the sea bottom is weak, so that normal-mode propagation is negligible. Thus, assuming that the target echo arrives at the horizontal array with the angle θ, the spacetime target echo signal along the array is expressed as

$$s_{\text{target}}(x, t; \tau) = A\cos(2\pi f_0(t - t_x) + \phi)\text{win}(t - t_x : 0, T), \tag{1}$$

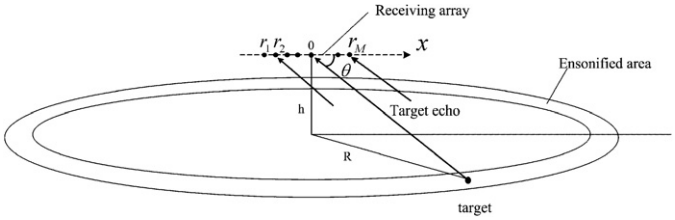

Figure 1. Schematic model of target detection in shallow water.

$$\mathrm{win}(t:0,T)=\begin{cases}1, & 0<t<T,\\ 0, & \text{otherwise.}\end{cases} \tag{2}$$

$$t_x=\tau-\frac{\cos\theta}{c}x, \tag{3}$$

where ϕ and A are the unknown or random phase and amplitude, respectively, c is the acoustic velocity, x is the coordinate along the array, and τ is the arrival time of the target echo. The receiving array with a length of L, as shown in figure 1, consists of M sensors $r_1, r_2, r_3, \ldots, r_M$, and the coordinate x at the middle of the array is taken as zero.

According to the point-scattering model [18], the interfering reverberation $R(x,t)$ can be treated as a sum of echoes scattered by the scatterers distributed at the ensonified cirque on the sea bottom, as shown in figure 1:

$$R(x,t)=\sum_{i=1}^{N(x,t)} a_i f(t-t_i(x),\mathbf{e}_i), \tag{4}$$

where $f(t)$ is the transmitted signal, a_i is the stochastic amplitude of the ith scattered signal, $t_i(x)$ is the stochastic arrival time of the ith scattered signal at the sensor with the coordinate x, and $N(x,t)$ is the number of scatterers that contribute to $R(x,t)$, itself a stochastic process. The $\mathbf{e}_i$ represents other stochastic parameters characterizing the scatterers (e.g., Doppler), and it is neglected in this paper for simplicity. Thus, the reflected signal of each individual scatterer has the same form of the transmitted signal, and thus has the same form of the target signal. The differences between individual scattered signals and target echoes lie in two facets. First, target echoes have different statistics (such as amplitude and phase) from those of the background scattered signals, and generally, target echoes are much stronger than the individual scattered signals. Second, there may be only one or several targets in the interested area, while there will be lots of scatterers, making the reverberation strong enough to conceal the target echo. Furthermore, the individual scattered signals come from different orientations with different time delays, which makes the reverberation have different spatial and temporal correlations from those of target echoes. For a single-frequency pulse signal, $R(x,t)$ has the horizontal spatio-temporal coherence form [18, 25–27]:

$$\rho_{\mathrm{R}}(x,\tau)\approx\begin{cases}J_0\left(\frac{2\pi|x|}{\lambda}\right)\left(1-\frac{|\tau|}{T}\right)\cos 2\pi f_0\tau, & -T<\tau<T,\\ 0, & \text{otherwise,}\end{cases} \tag{5}$$

where J_0 is the zero-order Bessel function, and λ is the wavelength of the transmitted signal.

Now, the problem is to decide whether there is a target echo embedded in the reverberation at the range R (or time τ)

$$\begin{cases}H_1: r(x,t)=s_{\mathrm{target}}(x,t;\tau)+R(x,t),\\ H_0: r(x,t)=R(x,t),\end{cases} \tag{6}$$

where $r(x, t)$ is the signal received by the array, and H_1, H_0 correspond to the two hypotheses that whether a target exists or not, respectively. As the target echo only exists during $[\tau, \tau+T]$, we let $\tau = 0$ for convenience and the decision is made according to the received signal $r(x, t)$ during $[0, T]$.

2.2. The conventional method

First we consider the binary case of a sine wave with random phase and amplitude in white Gaussian noise:

$$\begin{cases} H_1 : r(t) = A\sin(\omega t + \phi) + w(t), \\ H_0 : r(t) = w(t), \end{cases} \tag{7}$$

where $w(t)$ is the white Gaussian noise. Assuming that ϕ is uniformly distributed, the optimum receiver is [28]

$$l = L_c^2 + L_s^2 \underset{H_0}{\overset{H_1}{\gtrless}} \gamma, \tag{8}$$

where

$$L_c = \frac{2}{T}\int_0^T r(t)\cos(\omega t)\,\mathrm{d}t, \tag{9}$$

$$L_s = \frac{2}{T}\int_0^T r(t)\sin(\omega t)\,\mathrm{d}t. \tag{10}$$

The threshold γ can be determined for desired probability of false alarm P_{FA}. It is easy to prove that $\sqrt{l}$ is Rayleigh distributed under H_0 hypothesis, and $E(l|H_0) = 2E\left(L_c^2 \,\middle|\, H_0\right) = 2E\left(L_s^2 \,\middle|\, H_0\right) \triangleq \sigma^2$. Thus,

$$P_{\mathrm{FA}} = P(H_1|H_0) = \exp\left(-\frac{\gamma}{\sigma^2}\right). \tag{11}$$

The performance of such a receiver increases with the SNR A^2/σ^2 [28].

Now we turn back to the array signal in equation (6). To make the main lobe of the array centered at an angle θ, the signal received by the sensor at x is delayed by $\tau(x) = x\cos\theta/c$, and then all the delayed signals are summed up:

$$r(t) = \frac{1}{M}\sum_i^M r(x_i, t - \tau(x_i)) = A\cos(2\pi f_0 t + \phi) + \bar{R}(t), \tag{12}$$

where $\bar{R}(t) = (1/M)\sum_{i=1}^M R(x_i, t-\tau(x_i))$. The above equation is referred to as the spatial matched filter or commonly conventional beamforming [29].

Comparing equation (12) with the first equation in (7), the difference is between $\bar{R}(t)$ and $w(t)$. Although $\bar{R}(t)$ is not white and sometimes even not Gaussian, the optimal receiver in white Gaussian noise given by equation (8) is frequently used for its simple structure and good performance in most cases [30]. Thus, the conventional receiver for this problem is expressed by equations (8)–(12), and its structure is shown in figure 2(*a*).

2.3. The method based on PSR techniques

To utilize the PSR techniques, the SR system is inserted before the LCD [23]. First, the spatial component of the received signals $r(x) = A\cos(2\pi f_0 x\cos\theta/c + \phi) + R(x)$ is considered, and

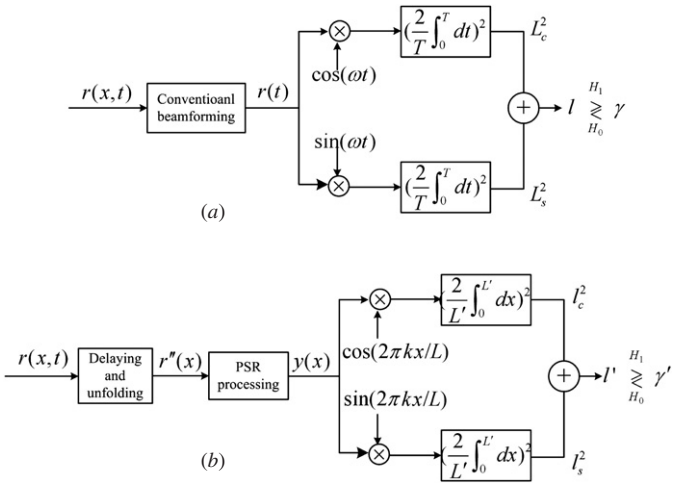

Figure 2. Block scheme of the two receivers. (*a*) Conventional receiver. (*b*) The receiver based on PSR techniques.

the signal at each sensor is delayed with $\tau_x = (L\cos\theta - k\lambda)x/(Lc)$ in the time domain to lower its spatial frequency:

$$r'(x,t) = r(x,t-\tau_x) = A\cos\left(2\pi f_0 t + \frac{2\pi k}{L}x + \phi\right) + R'(x,t), \tag{13}$$

where $R'(x,t) = R(x,t-\tau_x)$, and k is the number to be determined. Thus, its spatial component becomes $r'(x) = A\cos(2\pi kx/L + \phi) + R'(x)$, which is pre-processed by the SR system:

$$\frac{\mathrm{d}y}{\mathrm{d}x} = ay - by^3 + r'(x) = ay - by^3 + A\cos\left(\frac{2\pi k}{L}x + \phi\right) + R'(x), \tag{14}$$

where $a > 0, b > 0$ are the system parameters, and y is the system output. As we have assumed $x = 0$ at the middle of the array, there is $-L/2 \leqslant x \leqslant L/2$ in equations (13) and (14). For convenience in later expressions, we make the transformations, $x = x + L/2$ and $\phi = \phi - \pi k$, resulting in $0 \leqslant x \leqslant L$ in equations (13) and (14). Then, approximating the term $A\cos(2\pi kx/L + \phi)$ with a ladder function, that is, treating it as a constant value s_i in each interval $[(i-1)\Delta x, i\Delta x]$, and furthermore, approximating the term $R'(x)$ with Lorentzian colored noise [23], the approximated Fokker–Planck equation (FPE) related to equation (14) can be written as

$$\frac{\partial P_i(y,x)}{\partial x} = -\frac{\partial}{\partial y}[c_i(y)P_i(y,x)] + D\frac{\partial^2}{\partial y^2}\left[\frac{1}{1-d_x c_i'(y)}P_i(y,x)\right], \tag{15}$$

where $0 \leqslant x \leqslant \Delta x$, $P_i(y,x)$ is the probability density of the output y in the ith interval, $c_i(y) = ay - by^3 + s_i$, and $c_i'(y)$ is its derivative. D is the noise density of the approximated colored noise, and d_x is its correlation length, and they can be determined as $D = \sigma_{R'}^2/(4U_\mathrm{B})$, $d_x = D/\sigma_{R'}^2$, where $\sigma_{R'}^2$ is the variance of $R'(x)$ and U_B is the approximate bandwidth of reverberation's spatial frequency which is read from the Fourier transformation of the spatial coherence of $R'(x)$. We assume that variance of the reverberation has been normalized to 1, and hence, $d_x = D = 0.25/U_\mathrm{B}$.

In [23], the optimal LCD was designed according to the output statistics of equation (14) under both hypotheses. However, in this case the phase and amplitude of the target echo are both unknown or random, so the mean value of the output $\bar{y}(x)$ under H_1 hypothesis cannot be solved from the FPE, and the optimal LCD cannot be derived. For the target echo is periodic, it can be deduced that $\bar{y}(x)$ has the component of $A'\cos(2\pi kx/L + \phi')$ when the SR system reaches its cyclostationary state under H_1 hypothesis, and the phase ϕ' must be a function of both A and ϕ, while amplitude A' is only a function of A. Therefore, the conventional detector given in equations (8)–(10) still can be used for the output of equation (14):

$$l' = l_c^2 + l_s^2 \underset{H_0}{\overset{H_1}{\gtrless}} \gamma', \tag{16}$$

where

$$l_c = \frac{2}{L}\int_0^L y(x)\cos(2\pi kx/L)\,\mathrm{d}x, \tag{17}$$

$$l_s = \frac{2}{L}\int_0^L y(x)\sin(2\pi kx/L)\,\mathrm{d}x, \tag{18}$$

where L is the length of the receiving array. Denoting $E(l'|H_0)$ as σ'^2, now the crucial issue is to tune the system parameters a and b to maximize the output SNR, A'^2/σ'^2. For A is unknown or random here, we will consider the worst case that $A_{\min}$ is the minimum of the possible values, and then the system is designed for this worst case. For A' is independent of ϕ, given an arbitrary value of ϕ, A' can be solved from the cyclostationary solution of the FPE.

The solution of equation (15) can be obtained using the eigenfunction expansion method [31]:

$$P_i(y,x) \approx \sum_{n=0}^{\bar{N}} a_n^i \Phi_n^i(y)\exp\left(-\lambda_n^i x\right) + \left[P_{i-1}(y,\Delta x) - \sum_{n=0}^{\bar{N}} a_n^i \Phi_n^i(y)\right]\exp\left(-\lambda_{\bar{N}+1}^i x\right), \tag{19}$$

where λ_n^i is the nth eigenvalue of equation (15) in the ith interval, $\Phi_n^i(y)$ is the corresponding eigenfunction, and $a_n^i, n = 0, 1, \ldots, \bar{N}$, are constant coefficients. It is assumed that $0 = \lambda_0^i < \lambda_1^i \leqslant \cdots \leqslant \lambda_{\bar{N}+1}^i$, and λ_1^i is called the system response speed in the ith interval [13]. Thus with the given initial probability density function $P_1(y,0)$, $P_i(y,x)$ can be calculated from equation (19) recursively. Assume that s_i is periodic with number I (each period of the target echo is divided into I intervals), and thus, the system reaches its cyclostationary state when $P_{(i+I)}(y,\Delta x) = P_i(y,\Delta x) \triangleq \tilde{P}_i(y,\Delta x)$. Then, A' is derived from

$$A'^2 = \left[\frac{2}{I\Delta x}\int_0^{I\Delta x} \bar{y}(x)\cos\left(\frac{2\pi k}{L}x\right)\mathrm{d}x\right]^2 + \left[\frac{2}{I\Delta x}\int_0^{I\Delta x} \bar{y}(x)\sin\left(\frac{2\pi k}{L}x\right)\mathrm{d}x\right]^2, \tag{20}$$

where

$$\bar{y}(x) = \int_{-\infty}^{+\infty} y\tilde{P}_i(y, x-(i-1)\Delta x)\,\mathrm{d}y, \qquad (i-1)\Delta x < x \leqslant i\Delta x. \tag{21}$$

To determine σ'^2, the auto-correlation function of the output under H_0 hypothesis should be derived, that is, to solve the transition probability $P_0(y,x|y',0)$ under H_0 hypothesis, which obeys the same FPE:

$$\frac{\partial P_0(y,x|y',0)}{\partial x} = -\frac{\partial}{\partial y}[c_0(y)P_0(y,x|y',0)] + D\frac{\partial^2}{\partial y^2}\left[\frac{1}{1-d_x c_0'(y)}P_0(y,x|y',0)\right], \tag{22}$$

where $c_0(y) = ay - by^3$ and $c_0'(y)$ is its derivative. The solution can also be expanded as

$$P_0(y, x|y', 0) \approx \sum_{n=0}^{\bar{N}} a_n^0(y')\Phi_n^0(y)\exp\left(-\lambda_n^0 x\right) + \left[\delta(y - y') - \sum_{n=0}^{\bar{N}} a_n^0(y')\Phi_n^0(y)\right]\exp\left(-\lambda_{\bar{N}+1}^0 x\right). \tag{23}$$

Then we obtain the auto-correlation function of the output y under H_0:

$$C_y(x) = \iint yy' P_0(y, x|y', 0) P_0(y')\,\mathrm{d}y\,\mathrm{d}y', \tag{24}$$

where $P_0(y')$ is the stationary probability density function of the output under H_0. Based on this, σ'^2 is derived as

$$\sigma'^2 = \frac{4}{L^2}\iint \cos\left(\frac{2\pi k}{L}x\right) C_y(x - x')\cos\left(\frac{2\pi k}{L}x'\right)\mathrm{d}x\,\mathrm{d}x' + \frac{4}{L^2}\iint \sin\left(\frac{2\pi k}{L}x\right) C_y(x - x')\sin\left(\frac{2\pi k}{L}x'\right)\mathrm{d}x\,\mathrm{d}x'. \tag{25}$$

It is observed that for given values of $A_{\min}$ and k, the output SNR A'^2/σ'^2 is a function of a and b. Therefore, the system parameters a and b must be tuned properly to maximize $\mathrm{SNR}_{\mathrm{out}}(a, b)$. As the cyclostationary solution was used in equation (20), the system response speed should be fast enough to make the system reaches its cyclostationary state within few periods of the target signal. In [23], the value of $b = \bar{b}$ was first determined to satisfy the average system response speed under H_1 hypothesis when $a = 0$, and then a is optimized with $b = \bar{b}$ unchangeable. The same strategy of tuning parameters will be used here, while $\bar{b}$ is determined from $\lambda_1^0(0, \bar{b}) = 3k/L$, that is, to make the system response speed when $A_{\min} = 0$ be three times of the frequency of the target signal. For the system response speed increases with the value of A, this strategy will ensure the satisfaction of system response speed for the worst case. Then, the parameter a is optimized according to

$$\max_{a>0,\bar{b}} \mathrm{SNR}_{\mathrm{out}}. \tag{26}$$

Figure 3 plots some curves of $\mathrm{SNR}_{\mathrm{out}}$ versus a for different values of $A_{\min}$ when $k/L = 1/72$. It is found that $\mathrm{SNR}_{\mathrm{out}}$ is unimodal within a certain interested range of a, and a peak value of $\mathrm{SNR}_{\mathrm{out}}$ as well as the optimal a can be found for each value of $A_{\min}$.

To utilize the temporal component of the received signals, the two-dimensional signal $r'(x, t)$ in equation (13) is unfolded into longer one-dimensional signal:

$$r''(x) = r'\left(x - nL, \frac{nk}{f_0}\right) = A\cos\left(\frac{2\pi k}{L}x + \phi\right) + R'\left(x - nL, \frac{nk}{f_0}\right), \tag{27}$$

where $0 \leqslant x \leqslant L' = Tf_0L/k$, and $n = \lfloor x/L \rfloor$ is the floor number of x/L. Thus, $r'(x, t)$ is transformed into $r''(x)$ with a one-dimensional length of L'. We have shown that the smaller k is, the better the system performs [23], because the information in the temporal component of $r'(x, t)$ is more sufficiently utilized with smaller k. However, the smaller k is, the larger value L' takes, which increases the computational load. Moreover, when $k < 1/4$ the improvement on performance is limited. Therefore, $k = 1/4$ is adopted in this paper.

Now, the structure of the receiver based on PSR techniques can be drawn as figure 2(*b*). Note that $R'(x)$ in equation (14) is replaced by $R'(x - nL, nk/f_0)$ during execution, but the system is still designed according to equation (14) with $R'(x)$ of length L'. For some additional correlations are brought from the time domain into $R'(x - nL, nk/f_0)$, thus into

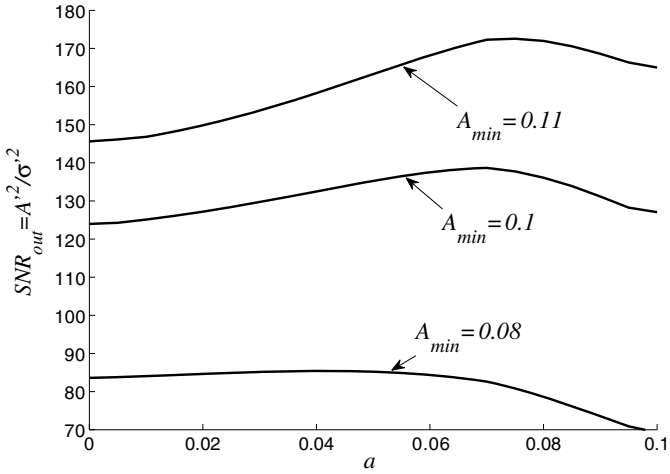

Figure 3. The relationship between $\mathrm{SNR}_{\mathrm{out}}$ and the parameter a, with $L = 1080$ and $k = 15$.

the output $y(x)$, σ'^2 derived from equation (25) should be modified. Denoting it as $\sigma_{\mathrm{m}}'^2$, the detailed deduction is given in the appendix. Substituting $\sigma_{\mathrm{m}}'^2$ into equation (11), one can get the threshold γ' of equation (16) for desired P_{FA}.

It is necessary to note that γ and γ' derived from equation (11) may not result in the desired probabilities of false alarm in practice, because the square roots of the outputs, $\sqrt{l}$ and $\sqrt{l'}$, are not Rayleigh distributed in most cases. Later, in the following section, we will find that the square root of the output of the conventional receiver $\sqrt{l}$ is not Rayleigh distributed even when $R(x, t)$ has the Gaussian density and Rayleigh envelope, because the spatial matched filter of equation (12) makes the probability of reverberation $\bar{R}(t)$ deviate from the Gaussian distribution. Besides, although $R'(x)$ is Gaussian, the output $y(x)$ is not Gaussian, and $R'(x - nL, nk/f_0)$ with different n are highly correlated, which increases the correlations of the output $y(x)$. Hence, conditions for the CLT ensuring the Gaussian and independent statistics of l_c and l_s are not satisfied, and $\sqrt{l'}$ is not Rayleigh distributed either.

3. Numerical simulation and results

3.1. Generation of reverberation

The first step of our simulation is to generate reverberation noise. Lots of work have been done on this topic [17, 24, 32]. Here we use the point-scatterer simulation method [20, 24], which simulates each scattered signal individually. Despite its inherent computational intensiveness, this method has direct control over the statistics of the scattering, thus the statistics of reverberation.

The geometry of reverberation simulation is shown in figure 4, which is the top view of figure 1. For $R \gg h$, the azimuth angles θ_i of the reflected signals are assumed to vary from 0 to 2π. In addition, we are interested in the range interval $[R - \Delta R_L, R + \Delta R_R]$, where $\Delta R_L + \Delta R_R = \Delta R \ll R$. Thus, the scatters are randomly placed on the sea bottom, with their position coordinates R_i and θ_i uniformly and independently distributed on $[R-\Delta R_L, R+\Delta R_R]$

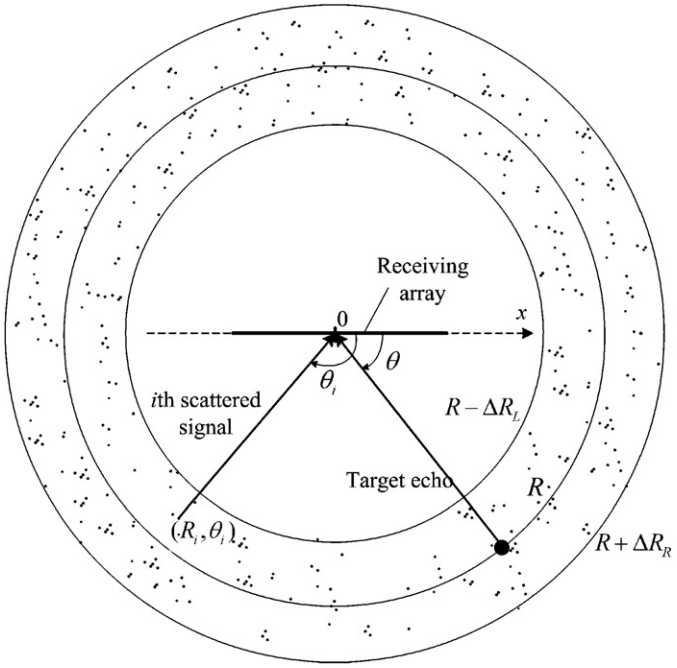

Figure 4. The geometry of simulation.

and $[0, 2\pi]$, respectively. To simulate the reverberation, each scattered signal is generated as

$$s^i_{\text{scat}}(x,t) = a_i \cos[2\pi f_0(t - t_i)]\text{win}(t - t_i : 0, T), \tag{28}$$

where

$$t_i = \frac{2(R_i - R) - x\cos\theta_i}{c}, \tag{29}$$

and a_i is assumed to be Rayleigh distributed. Here we have taken the time of the target echo (from the range R) arriving at the sensor with $x = 0$ as the zero-time-reference point. Thus, the total reverberation can be generated by

$$R(x,t) = \frac{1}{G}\sum_{i=1}^{N} s^i_{\text{scat}}(x,t), \tag{30}$$

where N is the total number of scatterers we set in the area, and G is a normalizing factor to ensure the unit variance of $R(x,t)$. For each sensor, the average number of scatterers that contribute to the reverberation at the same time, approximates $\langle N\rangle = (N/\Delta R)Tc/2$, where $N/\Delta R$ corresponds to the average number of scatterers distributed on the cirque with unit radial thickness. If each scattered signal has unit variance, there is $G = \sqrt{\langle N\rangle}$.

Therefore, for a given T, we can set $\langle N\rangle$ or $N/\Delta R$ large enough to make $R(x,t)$ have Gaussian distribution (or Rayleigh envelope), otherwise reduce $\langle N\rangle$ or $N/\Delta R$ to make $R(x,t)$ deviate from Gaussian distribution (or Rayleigh envelope). Figure 5 gives the estimated PDFs of an instantaneous value of $R(x,t)$ and its envelope for different values of $\langle N\rangle$. It can be found that when $\langle N\rangle$ is as large as 100, the PDFs of $R(x,t)$ and its envelope match well to the Gaussian and Rayleigh distributions, respectively, and when $\langle N\rangle$ is as small as 5, the PDFs of

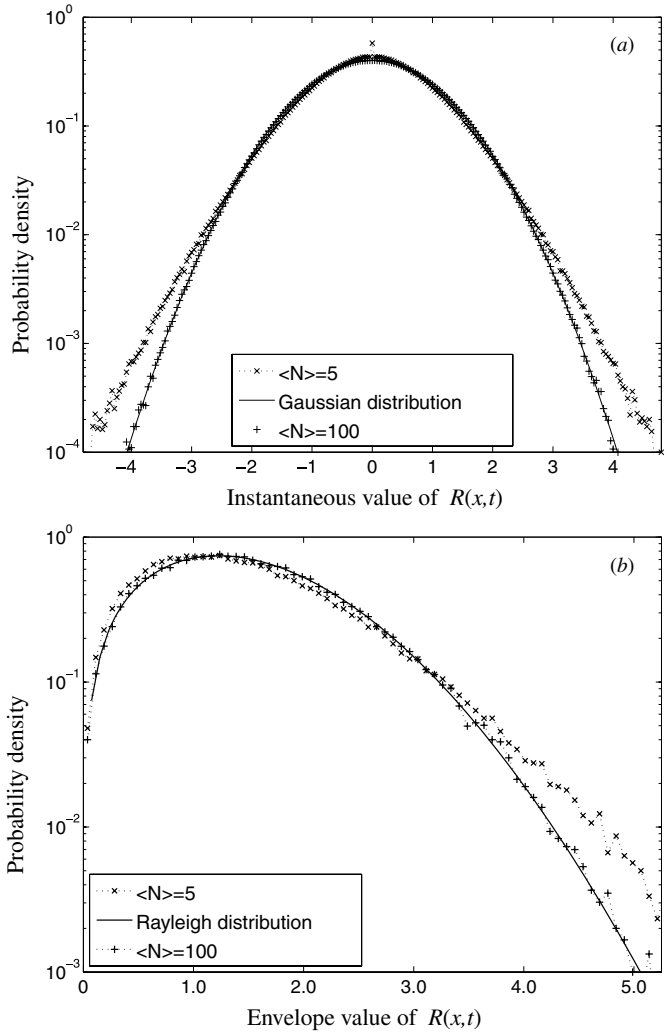

Figure 5. The PDFs of the reverberation $R(x, t)$ (panel (*a*)) and its envelope (panel (*b*)).

$R(x, t)$ and its envelope deviate from the Gaussian and Rayleigh distributions, respectively, with their tails increased.

3.2. Results and comments

Assume that the transmitter emits a pulse with frequency $f_0 = 15$ kHz and duration $T = 1$ ms. A target echo arrives at the array with azimuth angle $\theta = 60^\circ$. The signals are received by a horizontal sensor array with length $L = 18$ m and sensor interval $d = 0.05$ m. The amplitude of the target echo A is uniformly distributed on $[0.1, 0.2]$, and thus $A_{\min} = 0.1$.

First, the case of H_0 hypothesis (reverberation only) is studied to evaluate the actual probabilities of false alarm P_{FA}^a of the two receivers. To make it straightforward to compare the performances of the two receivers, the outputs l and l' are normalized respectively by σ^2 and

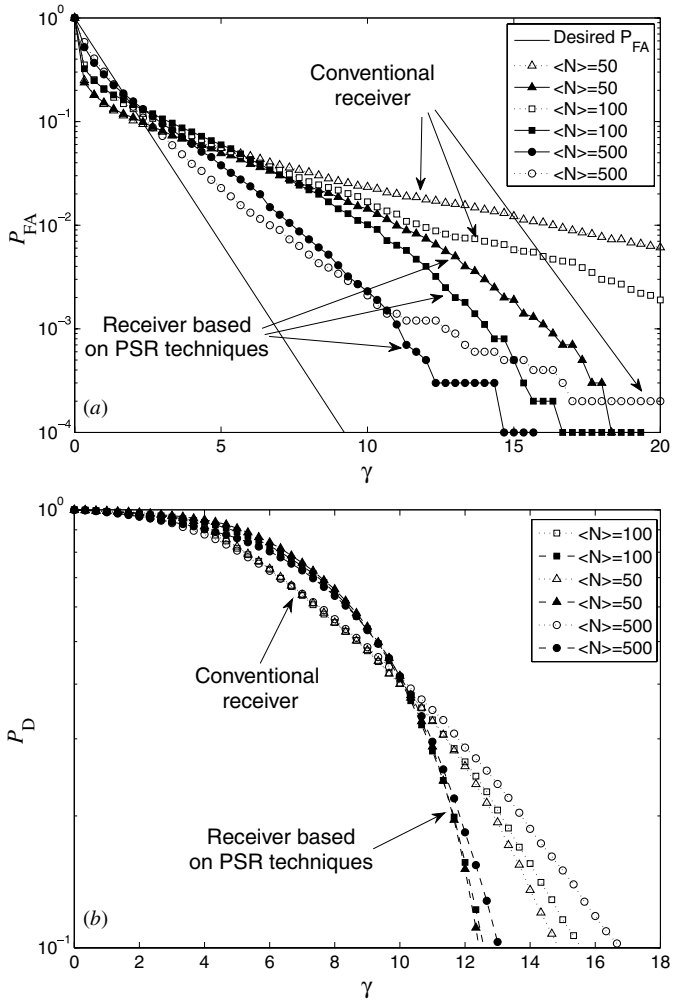

Figure 6. (*a*) The relationships between P_{FA}^{a} and γ of the two receivers for different values of $\langle N\rangle$. (*b*) The relationships between P_{D} and γ of the two receivers for different values of $\langle N\rangle$. Each curve is estimated from Monte Carol simulation with 10^4 realizations of the reverberation in each case.

$\sigma_{\mathrm{m}}'^2$ derived from equations (A.3) and (A.4), respectively. Figure 6(*a*) plots the relationships between P_{FA}^{a} and γ of the two receivers for different values of $\langle N\rangle$. Each curve of P_{FA}^{a} is estimated from Monte Carol simulation with 10^4 realizations of the reverberation in each case. The curve of desired P_{FA} is plotted according to equation (11) with $\sigma^2 = 1$. It is found that a given value of threshold γ, corresponding to a small desired probability of false P_{FA}, will result in larger actual probabilities of false P_{FA}^{a} of both the receivers, because $\sqrt{l}$ and $\sqrt{l'}$, the square roots of the outputs of the two receivers, are both non-Rayleigh distributed with heavier tails than Rayleigh distribution even when $\langle N\rangle$ is large, as shown in figure 7. Although it has been shown that when $\langle N\rangle = 100$ the reverberation of each sensor $R(x, t)$ has Rayleigh envelope (cf figure 5(*b*)), the beamforming of equation (12) makes the effective number of scatterers that contribute to $\bar{R}(t)$ at the same time much smaller than $\langle N\rangle$, which

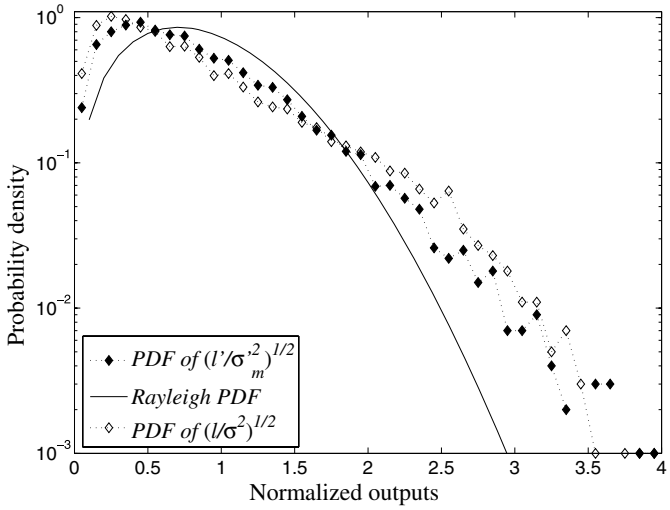

Figure 7. The PDFs of $\sqrt{l/\sigma^2}$ and $\sqrt{l'/\sigma_{\rm m}'^2}$, square roots of the normalized outputs of the two receivers, when $\langle N\rangle = 500$. Each curve is estimated based on 10^4 realizations.

makes $\bar{R}(t)$ have non-Gaussian PDF and non-Rayleigh envelope. Therefore, $\sqrt{l}$ is not exactly Rayleigh distributed even when $\langle N\rangle = 500$ (cf figure 7). Note that when $\langle N\rangle \to \infty$, $\sqrt{l}$ will have Rayleigh PDF, which however, is not considered here for its technical difficulties in numerical realization. As mentioned at the end of the last section, $\sqrt{l'}$ is not Rayleigh (cf figure 7), because the receiver based on PSR techniques is nonlinear, making its output $y(x)$ be non-Gaussian, and the correlations of $R'(x - nL, nk/f_0)$ at different n increase the correlations of the output, which violates the CLT that ensures the Gaussian and independent statistics of l_c and l_s. In addition, comparing the $P_{\rm FA}^a$ curves of the two receivers, for the cases of $\langle N\rangle = 50$ and $\langle N\rangle = 100$, the receiver based on PSR techniques has smaller $P_{\rm FA}^a$ than the conventional receiver in the region of large γ.

To evaluate the detection performance, only analyzing the cases under H_0 hypothesis is not sufficient. Then, the H_1 hypothesis is considered later. Similarly, 10^4 realizations of reverberation embedded with the target echo are generated independently, then processed by the two receivers, respectively. The outputs l and l' are also normalized by σ^2 and $\sigma_{\rm m}'^2$ respectively, then compared with the threshold γ, and thus the probabilities of detection $P_{\rm D} = P(H_1|H_1)$ can be estimated, which are shown in figure 6(*b*). It is found that $P_{\rm D}$ increases with $\langle N\rangle$ decreasing in the region of small γ for both receivers, while it decreases with $\langle N\rangle$ decreasing in the region of large γ for both receivers. Comparing the curves of the two receivers, the conventional receiver has higher $P_{\rm D}$ at large values of γ. However, in that region of γ, $P_{\rm D}$ is relatively small to make an efficient detection. It is more important that there is a region of γ (approximately from 4 to 10); the receiver based on PSR techniques has higher $P_{\rm D}$, and still in this region, it has almost equivalent or smaller $P_{\rm FA}^a$ than the conventional receiver when $\langle N\rangle \leqslant 100$, as shown in figure 6(*a*). That is to say there is such a region of γ, the receiver based on PSR techniques performs better than the conventional receiver when the number of scatterers is not very large.

Another intuitive measurement of the detection performance is the receiver operating characteristic (ROC) curve which is plotted as $P_{\rm D}$ versus $P_{\rm FA}^a$. From the ROC curve, one can find the corresponding $P_{\rm D}$ of a receiver for any given value of $P_{\rm FA}^a$. Figure 8 shows the

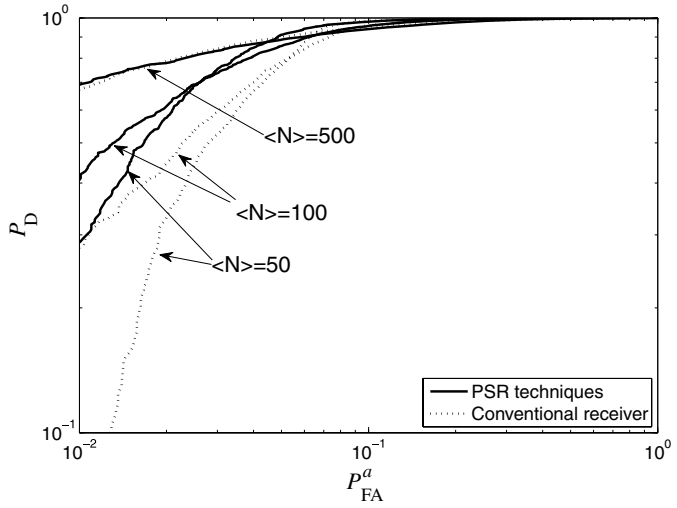

Figure 8. The ROC curves of the two receivers for different values of $\langle N \rangle$.

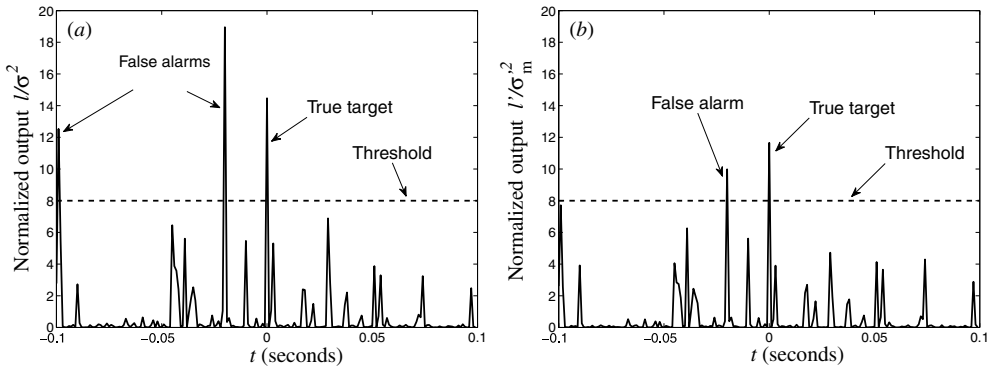

Figure 9. The temporal evolution of the normalized outputs of the two receivers during $[-0.1, 0.1]$ s, with a same snapshot $r(x, t)$ as their inputs. (*a*) Outputs of the conventional receiver. (*b*) Outputs of the receiver based on PSR techniques.

ROC curves of the two receivers for different values of $\langle N \rangle$. It can be seen that when $\langle N \rangle$ is relatively large, the ROC curves of the two receivers are close to each other, that is, they have nearly the same performance. And when the number of scatterers decreases, the performances of both receivers decrease, while the receiver based on PSR techniques performs better than the conventional receiver. Thus, it is proved again that in some conditions the conventional receiver can be improved by PSR techniques.

As an example, a snapshot of reverberation $R(x, t)$ from $t = -0.1$ s to 0.1 s was generated with $\langle N \rangle = 100$, and a target echo with $A = 0.2$ was embedded at time $t = 0$. Then the same snapshot of $r(x, t)$ was processed by the two receivers in figure 2, respectively. The temporal output evolutions of the two receivers, normalized by σ^2 and σ'^2_m, respectively, are shown in figure 9. Setting the threshold $\gamma = 8$, there are two false alarms for the conventional receiver, and only one false alarm after the PSR techniques was used. It can be seen that from the output

of the conventional receiver the true target position has been covered up by the high exceeding over the threshold due to the reverberation, and the high exceedings were suppressed by the PSR techniques, making the true target emerge.

In summary, it has been shown from our simulations that when the number of scatterers that contribute to the reverberation at the same time is not very large, the receiver based on PSR techniques will perform better and be more efficient for reverberation suppression than the conventional receiver.

4. Conclusions

In this paper, the problem of target detection in the presence of reverberation was considered, and the receiver based on PSR techniques for this detection problem was evaluated versus the conventional receiver. The reverberation is modeled according to point-scattering theory. Although the reverberation $R(x,t)$ has Gaussian PDF and Rayleigh envelope when the scatterer number is large, the square roots of the outputs of the two receivers, $\sqrt{l}$ and $\sqrt{l'}$, are both non-Rayleigh, resulting in higher probabilities of false alarm than the desired. Nevertheless, the results of numerical simulations show some advantages of the PSR techniques: when the number of scatterers that contribute to the reverberation at the same time is not very large, in a certain region of the threshold γ, the receiver based on PSR techniques has equal or smaller probabilities of false alarm but higher detection probabilities than those of the conventional receiver. That is to say, in some conditions, the receiver based on PSR techniques will perform better and be more efficient for reverberation suppression than the conventional receiver.

Acknowledgments

The authors greatly appreciate the support provided by the National Natural Science Foundation of China (no 10772161) and the National Natural Science Foundation for the Youth of China (no 60702022).

Appendix. Derivation of σ^2 and $\sigma_{\mathbf{m}}'^2$

According to equation (5), there is

$$\begin{aligned} e_{ij} &\triangleq E[r(x_i, t-\tau(x_i))r(x_j, t-\tau(x_j))|H_0] \\ &= \begin{cases} \sigma_R^2 J_0\left(\frac{2\pi\Delta x}{\lambda}\right)\left(1-\frac{\tau(\Delta x)}{T}\right)\cos 2\pi f_0\tau(\Delta x), & \tau(\Delta x) < T, \\ 0, \quad \text{otherwise}, \end{cases} \end{aligned} \tag{A.1}$$

where the variance of reverberation σ_R^2 is assumed to be normalized in this paper, $\tau(x) = x\cos\theta/c$, $\Delta x = |x_i - x_j| = |i-j|d$, and d is the sensor interval. Thus, the variance of $r(t)$ in equation (12) under H_0 hypothesis is

$$\sigma_{r(t)|H_0}^2 = \sigma_{\bar{R}}^2 = E[\bar{R}^2(t)] = \frac{1}{M^2}\sum_i\sum_j e_{ij}. \tag{A.2}$$

Again, according to equations (5), (8)–(10), there is

$$\begin{aligned} \sigma^2 = E[l|H_0] &= E\left[L_c^2 \,\middle|\, H_0\right] + E\left[L_s^2 \,\middle|\, H_0\right] \\ &= \frac{4}{T^2}\int_0^T\int_0^T \cos(\omega t)E[r(t)r(t')|H_0]\cos(\omega t')\,\mathrm{d}t'\,\mathrm{d}t \end{aligned}$$

$$
\begin{aligned}
&+\frac{4}{T^2}\int_0^T\int_0^T \sin(\omega t)\,E[r(t)r(t')|H_0]\sin(\omega t')\,\mathrm{d}t'\,\mathrm{d}t\\
&\approx \frac{4}{T^2}\int_0^T\int_0^T \cos(\omega t)\sigma_{\bar{R}}^2\left(1-\frac{|t-t'|}{T}\right)\cos[\omega(t-t')]\cos(\omega t')\,\mathrm{d}t'\,\mathrm{d}t\\
&+\frac{4}{T^2}\int_0^T\int_0^T \sin(\omega t)\sigma_{\bar{R}}^2\left(1-\frac{|t-t'|}{T}\right)\cos[\omega(t-t')]\sin(\omega t')\,\mathrm{d}t'\,\mathrm{d}t\\
&\approx \frac{2}{T}\sigma_{\bar{R}}^2\int_{-T}^T\left(1-\frac{|\tau|}{T}\right)^2\mathrm{d}\tau=\frac{4}{3}\sigma_{\bar{R}}^2. \qquad \text{(A.3)}
\end{aligned}
$$

When equation (27) is used as the input of system (14), the result of σ'^2, derived from the solutions of FPEs corresponding to equation (14) with $R'(x)$ of length L', should be modified. Divide $r''(x)$ and $R'(x)$ into Tf_0/k segments with each segment of length L, and then, in each segment $R'(x-nL, nk/f_0)$ and $R'(x)$ are statistically the same. In addition, σ'^2 is proportional to the length L' (when L' is larger than the correlation length of the output $y(x)$). Hence, the average contribution of each segment of $R'(x)$ to σ'^2 approximates $\sigma'^2/(Tf_0/k)$, and therefore, we can denote the average contribution of each segment of $R'(x-nL, nk/f_0)$ to $\sigma_{\mathrm{m}}'^2$ as $\sigma_L'^2=\sigma'^2/(Tf_0/k)$. However, $R'(x-nL, nk/f_0)$ in different segments are correlated according to equation (5), and the contributions of each segment $\sigma_L'^2$ are weighted together to $\sigma_{\mathrm{m}}'^2$ as

$$
\begin{aligned}
\sigma_{\mathrm{m}}'^2&=\sigma_L'^2\sum_{i,j=0}^{\frac{Tf_0}{k}-1}[\cos(2\pi ik)\rho_{ij}\cos(2\pi jk)+\sin(2\pi ik)\rho_{ij}\sin(2\pi jk)]\\
&\approx\frac{2k\sigma'^2}{Tf_0}\sum_{i,j=0}^{\frac{Tf_0}{k}-1}[\cos(2\pi ik)\rho_{ij}\cos(2\pi jk)], \qquad \text{(A.4)}
\end{aligned}
$$

where $\rho_{ij}=[1-|i-j|k/(Tf_0)]\cos[2\pi(i-j)k]$ is the coherence of $R'(x-iL, ik/f_0)$ (the ith segment) and $R'(x-jL, jk/f_0)$ (the jth segment). It is obvious that if $\rho_{ij}=\delta(i-j)$, $\sigma_{\mathrm{m}}'^2=\sigma'^2$ goes back to the case of $R'(x)$.

References

[1] Benzi R, Sutera A and Vulpiani A 1981 *J. Phys. A: Math. Gen.* **14** 453–7
[2] Nicolis C and Nicolis G 1981 *Tellus* **33** 225–34
[3] Gammaitoni L, Hanggi P, Jung P and Marchesoni F 1998 *Rev. Mod. Phys.* **70** 223–87
[4] Kiss L B 1996 *Chaotic, Fractal, and Nonlinear Signal Processing: AIP Conf. Proc* vol 375 ed R Katz pp 382–96
[5] Chapeau-Blondeau F 1999 *Int. J. Bifurcation Chaos* **9** 267–72
[6] Zozor S and Amblard P O 2002 *Signal Process.* **7** 353–67
[7] Duan F, Abbott D and Gao Q 2005 *Fluctuat. Noise Lett.* **5** L127–42
[8] Rousseau D, Anand G and Chapeau-Blondeau F 2006 *Signal Process.* **86** 3456–65
[9] Zozor S and Amblard P O 2003 *IEEE Trans. Signal Process.* **12** 3177–81
[10] Chen H, Varshney P, Kay S and Michels J 2007 *IEEE Trans. Signal Process.* **55** 3172–84
[11] Rousseau D and Chapeau-Blondeau F 2006 *Digit. Signal Process.* **15** 19–32
[12] Marchesoni F, Gammaitoni L and Bulsara A R 1996 *Phys. Rev. Lett* **76** 2609–12
[13] Xu B, Li J and Zheng J 2003 *J. Phys. A: Math. Gen.* **36** 11969–80
[14] Xu B, Duan F and Chapeau-Blondeau F 2004 *Phys. Rev.* E **69** 061110
[15] Zhang L, He J and Song A 2008 *Fluctuat. Noise Lett.* **8** L229–35
[16] Li J and Pan X 2007 *Mech. Syst. Signal Proc.* **21** 1223–32
[17] Etter P C 2003 *Underwater Acoustic Modeling and Simulation* 3rd edn (London: Spon)
[18] Olshevskii V V 1967 *Characteristics of Sea Reverberation* (New York: Consultants Bureau)
[19] Olshevskii V V 1978 *Statistical Methods in Sonar* (New York: Consultants Bureau)

[20] Alexandrou D, Demoustier C and Haralabus G 1992 *J. Acoust. Soc. Am.* **91** 1403–13
[21] Lyons A P and Abraham D A 1999 *J. Acoust. Soc. Am.* **106** 1307–15
[22] Abraham D A and Lyons A P 2002 *IEEE J. Ocean. Eng.* **27** 800–13
[23] Zhang H, Xu B, Jiang Z P and Wu X 2008 *J. Phys. A: Math. Theor.* **41** 105003
[24] Princehouse D W 1977 *Proc. IEEE Int. Conf. Acoustics, Speech, Signal Processing* vol 2 pp 827–35
[25] Cron B F and Sherman C H 1962 *J. Acoust. Soc. Am.* **34** 1732–6
[26] Urick R J and Lund G R 1970 *J. Acoust. Soc. Am.* **47** 109–11
[27] Jackson D R and Moravan K Y 1984 *J. Acoust. Soc. Am.* **75** 428–36
[28] VanTrees H L 1968 *Detection, Estimation, and Modulation Theory, Part:I. Detection, Estimation, and Linear Modulation Theory* (New York: Wiley)
[29] Manolakis D G, Ingle V K and Kogon S M 2000 *Statistical and Adaptive Signal Processing* (New York: McGraw-Hill)
[30] VanTrees H L 1971 *Detection, Estimation, and Modulation Theory, Part: III. Radar-Sonar Signal Processing and Gaussian Signals in Noise* (New York: Wiley)
[31] Li J and Xu B 2006 *Int. J. Bifurcation Chaos* **16** 427–35
[32] Abraham D A and Lyons A P 2004 *IEEE J. Ocean. Eng.* **29** 347–62